Association Aéronautique et Astronautique de France

55th 3AF International Conference on Applied Aerodynamics
12 — 14 April 2021, Poitiers – France

On the development of a turbulent boundary layer over staggered three dimensional cavities

Francesco Scarano[(1)], Romain Gojon[(1)] and Erwin R. Gowree[(1)]
[(1)]*ISAE-SUPAERO, Universite de Toulouse, 10 avenue Edouard Belin, 31055 Toulouse,*
erwin.gowree@isae-supaero.fr

February 22, 2021

ABSTRACT

Studies by Gowree et al. have suggested that staggered three dimensional circular cavities can potentially reduce the skin friction drag of a turbulent boundary layer developing over a flat plate. This is true up to a certain Reynolds number, after which the drag rapidly increases. The detailed mechanism behind the drag increase and the possible skin friction drag reduction was not discussed, due to the limitations in the measurement technique. In the current experimental campaign the results found by Gowree et al. have been confirmed, in addition, to more detailed insight of the turbulent boundary layer over the first rows of cavities. Through numerical simulations we aim to give a heuristic explanation of the two distinct behaviours. Here we report some quantitative evidence of the mechanism that may govern the drag increase, which is the main focus of the current study. The modification of the flow field in the presence of the cavities provides a qualitative explanation of the drag reduction benefit which is subjected for further investigation.

1. INTRODUCTION

Being the main contributor to the overall drag on an aircraft ($> 50\%$), skin friction drag has undergone serious scrutiny and is still a priority in the agenda for aerodynamic design and optimisation, especially in an era where there is an urge to reduce emissions. Let alone the difficulties in implementing technologies for skin friction drag reduction, the assessment of the skin friction drag penalty from a turbulent boundary layer itself is a complex task. Especially once the wall boundary conditions deviates from the hydrodynamically smooth condition and the well-established semi-empirical relations derived for turbulent boundary layers are no longer applicable. Perforated acoustic liners found in air-breathing engines is such an example. These surfaces, usually optimised for acoustic performances, can act to the detriment of the aerodynamic performance due to the significant rise in skin friction drag which results in pressure losses from the engine. The acoustic liners used in aeronautical applications are made of a perforated facing sheet which is placed on top a honeycomb cell sandwiched by a backing sheet. The primary flow is a turbulent boundary layer that develops over the facing sheet, where the perforations act to modify the flow in the near wall resulting in significant drag rise. There are still questions regarding the effect of the aero-acoustic interaction on the sharp drag rise which needs to be addressed.

With the aim of characterising the aerodynamic performances of the acoustic liners and give an insight of the flow field characteristics, it is fundamental to refer to the simpler case of a turbulent boundary layer grazing on a perforated surface with zero pressure gradient.

During an unpublished experimental campaign, E. Gowree observed that for lower Mach number, $M < 0.5$, the drag rise was less significant and in some cases it could even be lower than that on equivalent smooth and unperforated surfaces. This encouraged further low speed experiment by Gowree et al. [9] to investigate how the perforated surface or the presence of the 3D circular cavities could lead to a reduction in local skin friction drag. Over the past few decades, several techniques for skin friction drag reduction from turbulent boundary layer have been proposed. Longitudinal grooves known as riblets, inspired by the dermal denticles of sharks, have demonstrated the potential of skin friction drag reduction from turbulent

boundary layer, by rearranging the turbulent kinetic energy production cycle through modification of the wall boundary conditions. This technique was initially proposed by Walsh and co-workers and further detail of the flow physics was presented during the following studies [13, 15, 19, 4, 3, 7], to quote a few. In a more recent study van Nesselrooij [17] demonstrated that dimples could also reduce skin friction drag for certain Reynolds number regime and the physical mechanism was once again tied to the near wall production cycle modification. On the other hand, studies conduced on acoustic liners [20, 14] reported a skin friction drag increase. This behaviour is usually associated with an increase in the turbulent activity or rather an increase of the frequency of the bursts and ejections that contribute to an increase in the turbulent kinetic energy. The physical mechanism which governs this drag increase has not been sufficiently explained yet.

Hot wire measurements, coupled with an accurate determination of the wall to probe distance [10], showed, in correspondence with the first rows of cavities, a distortion in the average and root-mean-square velocity fields associated with a considerable oscillation of the boundary layer integral quantities. Even if the experimental results provide a real trend in drag in a more representative scenario, the measurement technique was limited in its ability to provide a detailed representation of the flow. Thus high fidelity Large Eddy simulations were conducted on a simplified geometry to complement and confirm the experimental finding. In this case we focused on the mechanism leading to the drag increase, but we were able, at the same time, to describe qualitatively a possible explanation of the drag benefit.

2. METHODS

2.1 Experimental setup

The experimental campaign has been conduced in the Sabre wind tunnel of ISAE-SUPAERO. The test models consisted in one smooth and one perforated surface, the geometrical characteristics of the latter will be reported above in the numerical setup. A Dantec P5517 hot wire probe for boundary layer attached to a two axes traversing system coupled with an optical probe to wall alignment technique [10], proved to be a reliable method to obtain velocity profiles at a close distance one another and to obtain measures close to the wall.

Along the center-line of the plate, and in correspondence to the first two rows of cavities, a series of velocity profiles with a fine spacing of 2.5 mm was made, Figure 1. This led to a 2D grid covering a region of the first two cavities where the distortion of the turbulent boundary layer is expected to be more pronounced.

2.2 Numerical setup

A high-order finite-volume code is used to solve the compressible Navier-Stokes equations. It solves the spatially filtered compressible Navier-Stokes equations for conservative variables using a finite volume formulation and a control-volume based discretization on unstructured hexahedral meshes. For time stepping, an explicit third-order Runge-Kutta scheme is used. For the spatial derivative, the solver uses a fourth-order non-dissipative centred numerical scheme [5]. The subgrid-scale model of Vreman [18] is used to dissipate the small scale turbulent structures that are not resolved by the mesh. We are thus performing explicit LES. This solver has been used previously for several studies of turbulent flow over an airfoil [1, 16] or shock boundary layer interaction [11, 12].

The simulations have been performed by changing the inlet condition in order to study the effect of the Reynolds number on the topology of the flow keeping fixed the geometry excluding the direction normal to the wall that is scaled with the boundary layer thickness. The wall resolved mean velocity profiles obtained experimentally have been used as inlet condition. The free-stream velocities, the boundary layer thickness at the inlet of the model δ_0, and the ranges of Reynolds number based on the momentum thickness along the model are summarized in the Table 1.

CASE	U_∞ [m/s]	δ_0 [m]	Re_θ
I	10	18.23×10^{-3}	1440 - 1830
II	15	18.76×10^{-3}	2230 - 2710
III	20	17.84×10^{-3}	2780 - 3380

Table 1: Boundary layer parameters imposed at the inlet of the domain.

Since the measurements were performed with a hot wire probe, only one component of the Reynolds stress is available (fluctuations of the stream-wise velocity). Therefore it has been decided then to assign the average turbulent velocity profile and study its effect on the topology of the flow. The lack of synthetic turbulence allows a reductions in the computational costs; this numerical approach has already been used for similar investigations [2].

We tried to reproduce, numerically, the experimental model that consisted of a face sheet with a grid of staggered circular cavities. During the experimental campaign we focused our attention on the first two rows of cavities where we saw a stronger effect on the turbulent boundary layer.

As a matter of fact, the numerical geometry consisted of three rows of cavity with a stagger angle of 45 deg and a spacing of L_c =22 mm as shown in Figure 2; the first row is located one diameter downstream of the inlet. A periodic boundary condition on the transverse direction

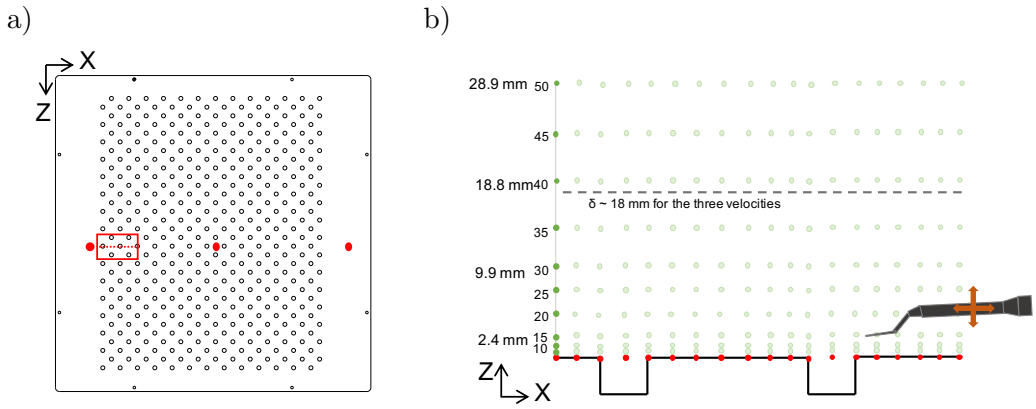

Figure 1: Experimental setup, a) perforated surface model (in red the measurements locations), b) side view of the 2D grid.

is assigned. The cavities have the same dimension and spacing of the experimental model, the thickness of the perforated surface was kept constant, providing a cavity depth t =4 mm, and so was the diameter of the perforation , $d = 5$ mm. This resulted in a ratio of diameter-to-depth, $d/t = 1.25$.

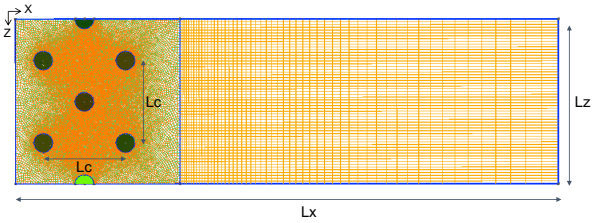

Figure 2: Numerical geometry and mesh, quad unstructured mesh around the cavities.

The geometry and grid parameters used for the present investigation are presented in Table 2 where X is the longitudinal coordinate, Y is the wall normal coordinate, and Z is the transverse coordinate. The domain was divided in two parts, the first one goes from the inlet up to $2L_c$ while the second goes up to the outlet. The dimensions are reported in Table 2. An unstructured grid for the first part and a structured grid for the second one were generated, the reason for this choice being the simplification of the meshing procedure when dealing with the cavities. On the second part of the mesh an increasing cell size factor of 1.05 is assigned in order to have the last cells to behave like a sponge region.

The grid consists of about 6 millions hexahedral cells. Those grids are designed from surface grids at the plate extruded in the wall normal direction. At the wall, a cell size of $\Delta y = 1.38 \times 10^{-}5$ m is imposed in order to have $y^+ \approx 1$ at the wall. In the region 0 to δ, the mesh size increases by a factor 1.10, then by a factor 1.25 from δ to 2.5δ, and finally a sponge zone with cells increasing in size by a factor 1.35 is used up to 4δ.

L_x/Lc	L_y/δ	L_z/Lc
6.5	4	2

Table 2: Geometry dimensions, with δ the boundary layer thickness imposed at the inlet of the domain and L_c distance between the cavities.

3. RESULTS AND DISCUSSIONS

3.1 Experimental results

Single profiles taken at the leading edge and trailing edge of both the perforated and the smooth surface allowed the determination of the skin friction by means of momentum deficit. The measurements taken on the smooth surface validated the technique showing a good match with the Colels-Fernholz relation for smooth walls, Figure 3. For the perforated wall a non-negligible decrease in skin friction drag, 12% and 7%, was observed for the case of 10 m/s and 15 m/s respectively when compared with the smooth case and a sudden rise of 13% was observed at 20 m/s.

From the velocity profiles, it is possible to evaluate the percentage variation between the momentum thickness of the perforated and smooth wall with the Reynolds number based on the cavity diameter.

The results reported in Figure 4 confirmed the findings of Gowree et al. [9] by consolidating the fact that the momentum thickness, which also represents the skin friction drag, is strongly correlated with the Reynolds number based on cavity diameter. This consolidates the initial arguments laid by Gowree et al. regarding the two distinct regime based on Re_d, one being of drag reduction and the other of drag increment when compared with a smooth surface.

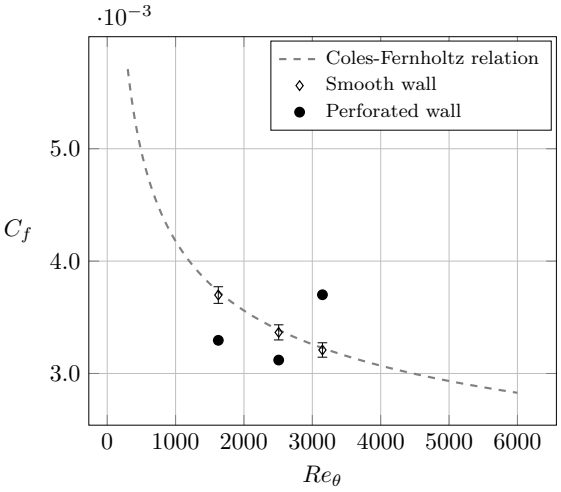

Figure 3: Friction coefficient for smooth and perforated model, comparison with Coles-Fernholtz relation valid for smooth walls.

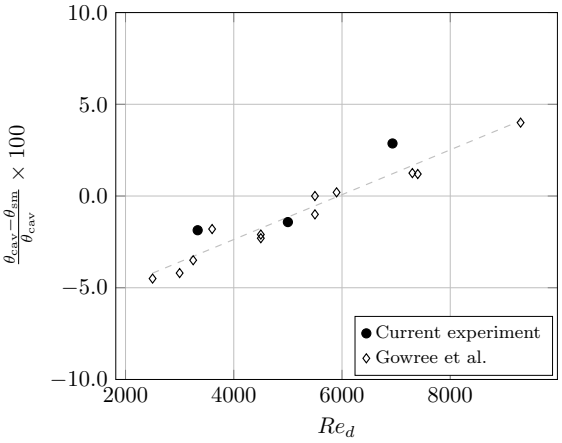

Figure 4: Momentum thickness percentage variation between perforated and smooth surface, measurements taken at the trailing edge of the model, comparison with Gowree et al. [9] and linear trend with Reynolds based on the diameter of the cavity.

From a further interpolation of the 2D grid measurements, the contour of the mean velocity and root mean square was obtained as reported in Figure 6 for the 15 m/s case. A distortion of the boundary layer is already evident just from the mean flow contour in Figure 6. This effect was accentuated in the U_{RMS} fields where there spatial development of the flow appears to be oscillatory. This distortion is even more evident if we consider the evolution of the integral boundary layer quantities along the two rows of cavities. In particular, for the three free-stream test velocities, the evolution of the momentum thickness is reported in Figure 5 together with five terms Fourier series that approximate the trends.

The oscillations appear to be of smaller amplitude for

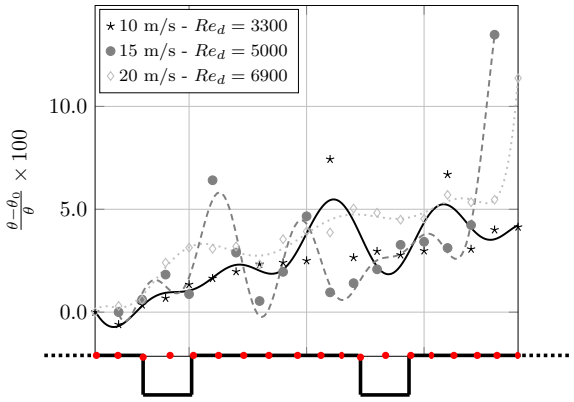

Figure 5: Percentage evolution of the momentum thickness along the first two rows of cavities for the three velocities tested.

the 20 m/s case but they start right downstream of the first cavity. For the 15 m/s and 10 m/s cases the oscillations start gradually with a relative peak that is slightly downstream respect the 20 m/s case. Both the 20 and 15 m/s cases have a sudden increase in the momentum thickness that could suggest a breakdown of the mean flow that does not seem to be present in the case of the 10 m/s case.

These experimental results were very insightful in understanding the major modification that the mean flow undergoes in the vicinity of the leading cavities. The considerable distortion with increasing free-stream velocity or Re_d is in line with the two regimes of Re_d identified earlier, where the critical regime can be define as that experiencing an increase in momentum thickness, thus skin friction drag. Usually, a critical Reynolds number will be linked to a change of flow behaviour through a transition or breakdown process. The jump in the momentum thickness demonstrates this behaviour, however the restrictive nature of the experimental results cannot provide a larger picture of the breakdown process, hence complementary LES simulations was undertaken.

3.2 Numerical results

For the numerical results we mainly focused on the comparison between the 10 and 20 m/s cases. A first qualitative view of the structures produced by the cavities is presented in Figure 7. From the Q-criterion, the formation of semi-circular structures in correspondence to the first row of cavities is visible, but the the structures appear to increase in intensity for the 20 m/s case. When the flow encounters the circular cavity, a 3D effect is intrinsically produced. The flow enters inside the cavities and a self-sustaining recirculation region is created. The first consequence is a jetting at the downstream part of the cavities with a positive velocity normal to the wall out of

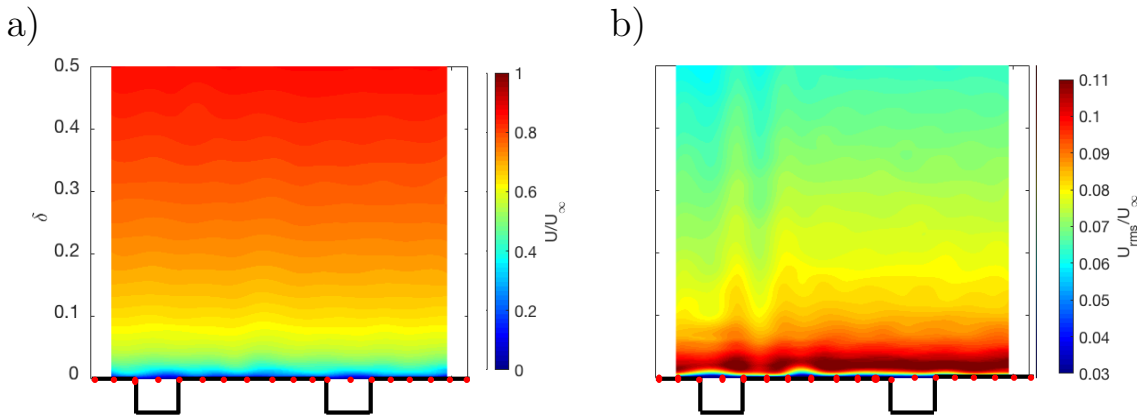

Figure 6: Distortion in the non dimensional mean velocity and U_{RMS} field at 15 m/s, interpolation of hot wire measurements.

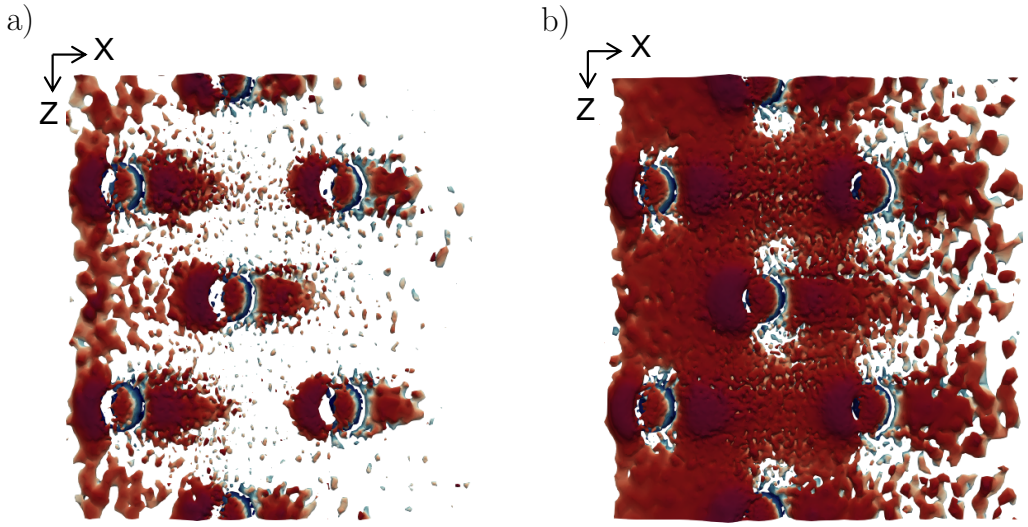

Figure 7: Iso-surface of the Q-criterion, comparison of a) 10 m/s and b) 20 m/s case.

the cavity. In Figure 8 the normal to wall velocity is reported for the 20 m/s case, the values and the topology for the 10 m/s differs only slightly. We can notice that the jetting is more pronounced for the cavity at the first row and it is attenuated in the second row.

The second phenomenon is the spillage of flow over the sides; this latter generates an alternating span-wise velocity pattern visible in Figure 9 which shows a slice at $\frac{Y}{\delta} = 0.01$ of the contour of the non dimensional span-wise mean velocity. This phenomenon is present for the three inflow conditions tested. The magnitude of this lateral velocity, evaluated at a fixed value of Y/δ, is of the order of 1% of the free-stream velocity. We identified a decreasing trend of the non-dimensional side velocity with the free-stream velocity and we estimated a decrease of 13% passing from 10 to 20 m/s.

In the Figure 10 a comparison of the magnitude of the total $U_{\mathrm{RMS}}/U_{\infty}$ is presented. The scale of the contour for the 20 m/s case is ten times larger than the one of 10 m/s. We can then notice immediately that inside the cavity, for the 20 m/s case, the fluctuations are larger compared to the 10 m/s case. For both free-stream velocities we can notice an effect of the first cavity to the second one, in fact the U_{RMS} is larger inside the cavity on the second row. In addition, for the 20 m/s case we can notice that the U_{RMS} increases even in the region downstream the second cavity close to the wall.

The profiles taken experimentally on the smooth part right after the first and the second cavities confirm that this effect is indeed more pronounced for the 20 m/s case, Figure 11. We stress again here that the U_{RMS} in the simulation is purely due to the presence of the cavity and not to the free-stream turbulence, as no synthetic turbulence was injected at the inlet.

Figure 8: Jetting phenomenon, contour of U_Y/U_∞ at 20 m/s, slice normal to the wall at $Y/\delta = 0.01$.

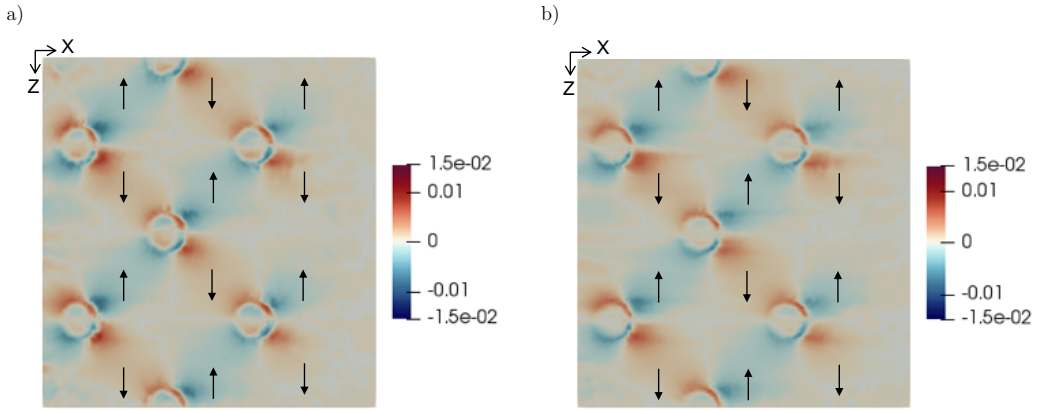

Figure 9: Span-wise flow pattern, contour of U_Z/U_∞ a) 10 m/s b) 20 m/s case, slice normal to the wall at $Y/\delta = 0.01$.

Figure 10: Magnitude of U_{RMS}, comparison and a) 10 m/s and b) 20 m/s.

In Figure 12 a comparison of the U_{RMS} of the stream-wise component is reported for the cases 10 and 20 m/s. The contours show a slice from the top taken at $Y/\delta = 0.01$. One can notice a rearrangement of the flow in the cavities both passing from 10 to 20 m/s and passing from the first to the second row. For the second row at 20 m/s the rearrangement is evident with the formation of three distinguishable lobes that suggest the presence of coherent structures inside the cavities.

On the experimental turbulent spectra at 20 m/s, downstream the second cavity, we noticed a sharp peak at a Strouhal number around $Sr = 0.3$ where $Sr = \frac{\hat{f}t}{U_\infty}$. Using a numerical probe at the same position we were able to retrieve a similar peak in the numerical spectra of the average stream-wise velocity component at $Sr \cong 0.29$, as it is visible in Figure 13. This would suggest we correctly captured a modulation of the mean flow due to the first rows of cavities.

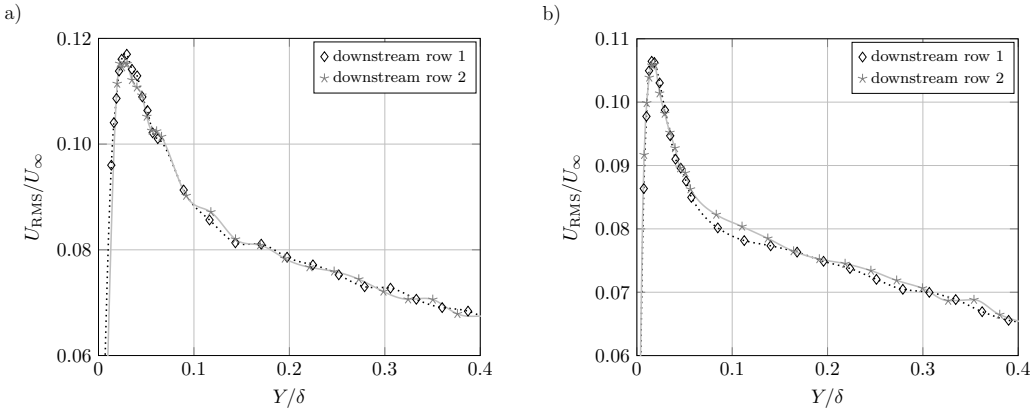

Figure 11: Experimental U_{RMS} of stream-wise velocity taken after the first and second cavity, comparison and a) $10\,\mathrm{m/s}$ and b) $20\,\mathrm{m/s}$.

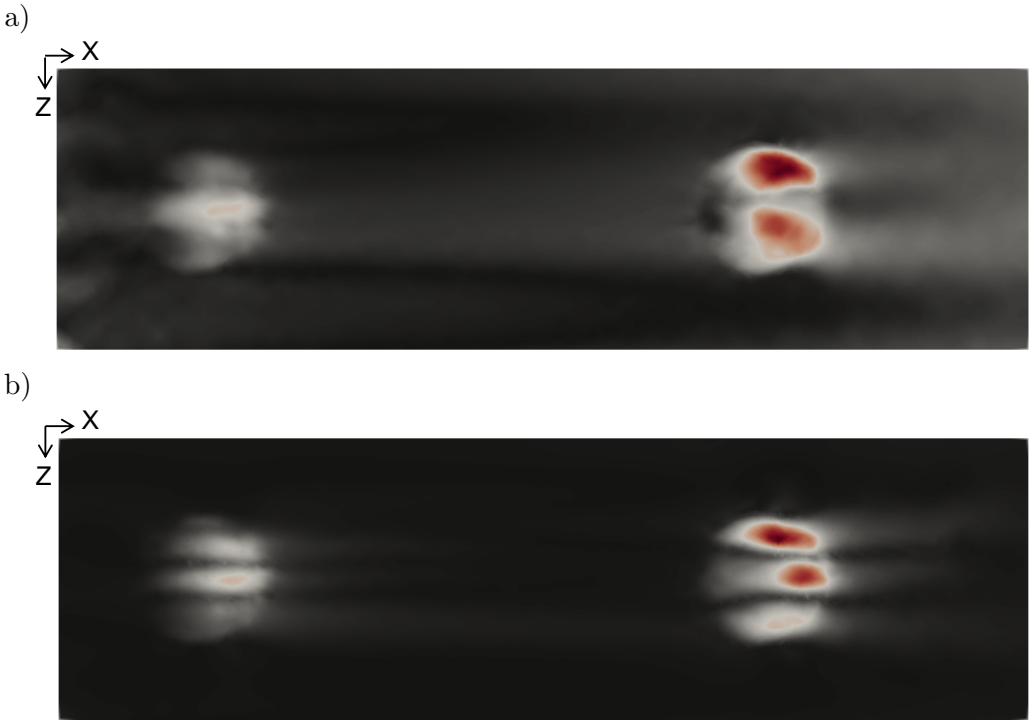

Figure 12: Top view of U_{RMS} of stream-wise velocity taken after the first and second cavity, comparison and a) $10\,\mathrm{m/s}$ and b) $20\,\mathrm{m/s}$, slice normal to the wall at $Y/\delta = 0.01$.

This is further confirmed when looking at the wavelength of the oscillation obtained by an FFT on the stream-wise velocity at a fixed location of Y/δ along the stream-wise direction. In both the numerical and experimental case we can clearly see a peak at around 1.3 times the diameter of the cavity and a second one at 2.4, Figure 14.

3.3 Discussion

Based on the experimental results that confirmed Gowree's findings and hypothesis, two different regimes, depending on the Reynolds number could potentially be identified: the "drag benefit regime" in which the cavities seem to produce a beneficial effect for the skin friction and a regime in which the skin friction increases, the "drag penalty" regime. We aim here to provide an explanation of the possible mechanism that governs these two behaviours while relying on the flow topology that arises from the numerical results.

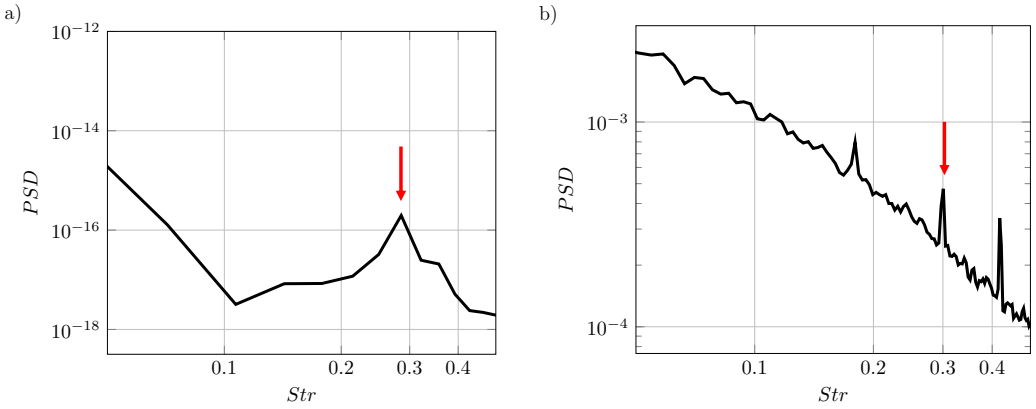

Figure 13: Power Spectral Density for 20 m/s, a) LES simulation b) experiment; probes located downstream of the second cavity at $Y/\delta = 0.01$.

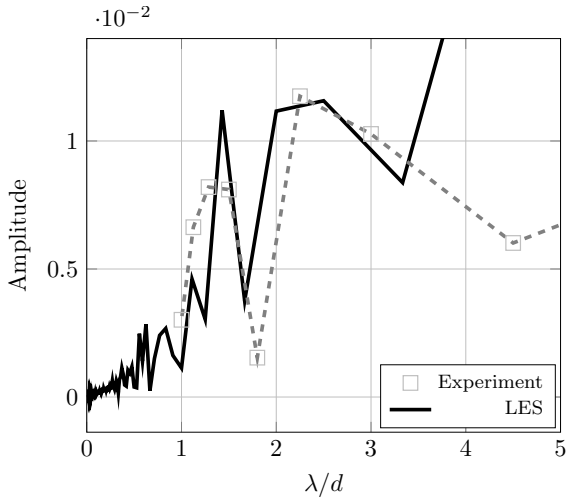

Figure 14: FFT of the spatial oscillation of the stream-wise velocity along the first two cavities, $Y/\delta = 0.01$, comparison between experiment and numerical simulation.

We identified a span-wise velocity pattern between the cavities that matches quite well with the drag benefit explanation given by van Nesselrooij for staggered dimples. They postulated, in fact, that staggered dimples are able to create an alternating span-wise velocity pattern which is the cause of of a reduction in turbulence induced friction. They stressed the importance of the staggered configuration and the strong interaction between the dimples.

According to this hypothesis, the flow, when passing between the cavities in the inner layer, is subjected to an alternating span-wise velocity. It could then be confined in span-wise direction to follow a particular path, in other words the span-wise velocity would act as if it was a physical constraint. This mechanism could potentially reduce the span-wise movement and propagation of rolls and could weaken the sweep and the burst activity, responsible for turbulent kinetic energy production in the boundary layer. The final consequence of this process would be the reduction in skin friction found experimentally. A similar mechanism is indeed the one of the riblets, but what is described here has potentially a closer resemblance with drag reduction trough span-wise wall oscillation described by Karniadakis [8] and Yakeno [21]; the wall oscillation in fact generates a span-wise velocity that hinders the rolls and reduces the hairpin vortex activity.

According to van Nesselrooij the drag coefficient decreases with the Reynolds number while in our case we notice a clear increasing trend. This can be ascribed to the different geometry considered (shallow dimples versus circular cavities); in addition, in our case another mechanism can play an important role in counteracting the drag benefit and produce a drag increase.

On the other hand, in fact, the sudden increase of skin friction at 20 m/s can be explained as an effect of the breakdown of the turbulent structures created by the cavities. The Reynolds number dependence may suggest that the cause of this may be an instability mechanism generated by the cavities.

At this purpose it is very interesting to underline the similarities between our results and the results reported by Brès and Colonius [6]. They investigated square cavities of infinite span-wise dimension and different length to depth ratio $\left(\frac{d}{t}\right)$.

A stability analysis assessed the presence of a 3D centrifugal instability. For cavities with $1 < \frac{d}{t} < 2$ they found an unstable mode at a Strouhal number around 0.31. Even without performing a stability analysis we were able to assess both in the experimental and numerical results an oscillation characterized by similar values of Strouhal number. In addition to that, the arrangement of the flow in lobes that we identified in the contour of stream-wise U_{RMS} have close resemblance with the structures inside the cavity described by Brès and Colonius which are an

expression of the aforementioned instability.

For all the velocities we noticed a strong influence of the first cavity on the second one: the disturbances produced by the first cavity interfere with the second cavity and this leads to a partial rearrangement of the flow and an increase in turbulence activity. We may infer that this instability, in some cases, when the modes are amplified up to a certain level, is the cause of the occurrence of the aforementioned break of the structures. This can explain the drag increase found experimentally and the increase in U_{RMS} shown before.

4. CONCLUSION & FURTHER WORKS

Within reasonable confidence, coupling experimental and numerical results, we demonstrated the presence of a distortion and oscillation of the mean flow field of a turbulent boundary layer caused by the presence of circular cavities in staggered arrangement. We presented here some evidence of an instability mechanism that could govern this oscillation and, in certain conditions, be responsible for the drag increase found experimentally.

To summarize, the intrinsically three-dimensionality of the case studied may generate a span-wise flow pattern and an instability mechanism. Finally the overall effect on drag will be a balance between these two effects. In some cases the flow results to be stable or the instability does not produce any modification in the turbulent structures and so the overall effect is beneficial for the skin friction; when the instability occurs it can overcome the effect of the span-wise flow enhancing the burst and leading to a skin friction increase.

A stability analysis will be necessary in order to provide more quantitative evidences of the instability mechanism that we think governs the drag increase for certain flow regimes; this should bring to a more precise evaluation of a critical Reynolds number. In addition, the application of methods such as proper orthogonal decomposition and dynamic mode decomposition should better reveal the arrangement of the structures generated by the cavities. Furthermore, with these techniques it should be possible to detect modes that contribute to the increase in turbulent kinetic energy production and how these affect the skin friction drag.

On parallel, more quantitative investigations are planned in order to generate further insight into the drag reduction mechanism and to confirm the hypothesis described here and reported in the literature.

5. ACKNOWLEDGEMENTS

The authors thank the AID (Agence Innovation Défense) for their financial support to the FriDA project. This work was performed using HPC resources from GENCI-IDRIS and GENCI-CINES on Jean Zay, Occigen (Grant A0082A07178) and CALMIP on Olympe (Grant 2020-p1425).

REFERENCES

[1] Grebert A., Bodart J., and Joly L. Investigation of wall-pressure fluctuations characteristics on a naca0012 airfoil with blunt trailing edge. In *22nd AIAA/CEAS Aeroacoustics Conference*, page 2811, 2016.

[2] Michael Bauerheim and Laurent Joly. Les of the aero-acoustic coupling in acoustic liners containing multiple cavities. In *AIAA aviation forum 2020*, 06 2020.

[3] D. W. Bechert, M. Bruse, and W. Hage. Experiments with three-dimensional riblets as an idealized model of shark skin. *Experiments in Fluids*, 28(5):403–412, 2000.

[4] D. W. Bechert, M. Bruse, W. Hage, J. G. T. van der Hoeven, and G. Hoppe. Experiments on drag-reducing surfaces and their optimization with an adjustable geometry. *Journal of Fluid Mechanics*, 338:59–87, 005 1997.

[5] I. Bermejo-Moreno, L. Campo, J. Larsson, J. Bodart, D. Helmer, and J.K. Eaton. Confinement effects in shock wave/turbulent boundary layer interactions through wall-modelled large-eddy simulations. *Journal of Fluid Mechanics*, 758:5–62, 2014.

[6] Guillaume A. Brès and Tim Colonius. Three-dimensional instabilities in compressible flow over open cavities. *Journal of Fluid Mechanics*, 599:309–339, 2008.

[7] B. Dean and B. Bhushan. Shark-skin surfaces for fluid-drag reduction in turbulent flow: a review. *Philosophical Transactions of the Royal Society of London A: Mathematical, Physical and Engineering Sciences*, 368(1929):4775–4806, 2010.

[8] Karniadakis G. E. and Choi K.S. Mechanisms on transverse motion in turbulent wall flows. *Annual Review of Fluid Mechanics*, 35(1):45–62, 2003.

[9] E.R. Gowree, C. Jagadeesh, and C.J. Atkin. Skin friction drag reduction over staggered three dimensional cavities. *Aerospace Science and Technology*, 84:520–529, 2019.

[10] Erwin Gowree, Chris Atkin, and S Gruppetta. A simple digital-optical system to improve accuracy of hot-wire measurements. *Measurement Science and Technology*, 26, 09 2015.

[11] A. Grébert, J. Bodart, S. Jamme, and L. Joly. Simulations of shock wave/turbulent boundary layer interaction with upstream micro vortex generators. In *10th International Symposium on Turbulence and Shear Flow Phenomena*, number 2B-2, Jul. 2017.

[12] A. Grébert, J. Bodart, S. Jamme, and L. Joly. Simulations of shock wave/turbulent boundary layer interaction with upstream micro vortex generators. *International Journal of Heat and Fluid Flow*, 72:73–85, Aug. 2018.

[13] Walsh M. J. Drag characteristics of v-groove and transverse curvature riblets. *Progress in Astronautics and Aeronautics*, 72:168–184, August 1980.

[14] Christopher Jasinski and Thomas Corke. Mechanism for increased viscous drag over porous sheet acoustic liners. *AIAA Journal*, 0(0):1–12, 0.

[15] Choi K.S. Near-wall structure of a turbulent boundary layer with riblets. *Journal of Fluid Mechanics*, 208:417–458, 11 1989.

[16] Boukharfane R., Bodart J., Jacob M.C., Joly L., Bridel-Bertomeu T., and Node-Langlois T. Characterization of the pressure fluctuations within a controlled-diffusion airfoil boundary layer at large reynolds numbers. In *25th AIAA/CEAS Aeroacoustics Conference*, 2019.

[17] M. van Nesselrooij, L. L. M. Veldhuis, B. W. van Oudheusden, and F. F. J. Schrijer. Drag reduction by means of dimpled surfaces in turbulent boundary layers. *Experiments in Fluids*, 57(9):142, Aug 2016.

[18] A.W. Vreman. An eddy-viscosity subgrid-scale model for turbulent shear flow: Algebraic theory and applications. *Physics of fluids*, 16(10):3670–3681, 2004.

[19] Bechert D. W. and Bartenwerfer M. The viscous flow on surfaces with longitudinal ribs. *Journal of Fluid Mechanics*, 206:105–129, 009 1989.

[20] S. Wilkinson. Influence of wall permeability on turbulent boundary-layer properties. In *AIAA 21st Aerospace Sciences Meeting*, 02 1983.

[21] Aiko Yakeno, Yosuke Hasegawa, and Nobuhide Kasagi. Modification of quasi-streamwise vortical structure in a drag-reduced turbulent channel flow with spanwise wall oscillation. *Physics of Fluids*, 26(8):085109, 2014.